Available online at www.sciencedirect.com
SCIENCE DIRECT®
Journal of Sound and Vibration 260 (2003) 237–263
JOURNAL OF SOUND AND VIBRATION
www.elsevier.com/locate/jsvi

Vibration characteristics of a cantilever plate with attached spring–mass system

M. Chiba[a,*], T. Sugimoto[b]

[a] *Department of Mechanical Engineering, Faculty of Engineering, Iwate University, 4-3-5 Ueda, Morioka 020-8551, Japan*
[b] *Honda R & D Co., Ltd, Tochigi R&D Center, Tochigi 321-3393, Japan*

Received 29 October 2001; accepted 29 April 2002

Abstract

Coupled free vibration analysis has been performed on a cantilever thin plate carrying a spring–mass system attached on an arbitrary point by using Rayleigh–Ritz method. Influence of an attached 'spring–mass' system, i.e., attached position, relative values of mass and spring constant, on the coupled vibration characteristics of the system has been clarified comparing with those of uncoupled ones. Optimal attached position to maximize coupled plate natural frequency is also investigated and shown in contour diagrams. The influence of an attached mass has also been investigated, as the limiting case whereby the spring stiffness of the 'spring–mass' system approaches infinity.

1. Introduction

Dynamic analysis of structures is indispensable in their safety design for earthquakes, fatigue and environmental problem such as noise. The structure is usually modelled as uniform plate or shell, however, in practice, it has varying thickness, or non-uniform material property, or it is locally stiffened, or is added to another part, or is connected with other structures. Then, a more realistic model has been investigated, i.e., as a structure which has added mass, added constraints, or added sub-dynamical system.

Among these studies on beams, as a simplest structural component, Young [1] treated a beam with mass, spring and dashpot. Laura et al. [2] studied free and forced vibrations of a simply supported beam and a rectangular plate carrying elastically mounted mass. Dowell [3] studied general properties of a combined dynamical system, in which he treated three examples, i.e.,

*Corresponding author. Tel.: +81-19-621-6404; fax: +81-19-621-6404.
E-mail address: mchiba@iwate-u.ac.jp (M. Chiba).

0022-460X/03/$ - see front matter
PII: S0022-460X(02)00921-5

simply supported beam with mass which is supported by spring, simply supported beam with spring–mass system, and two beams crossing crosswise. Nicholson and Bergman [4] considered a cantilever beam which is supported by mass–spring systems at some points, or to which some mass–spring systems are added. They used the Green function method to obtain natural frequency equation. Rossi et al. [5] treated Timoshenko beam with both simply supported, simply supported-clamped, and both clamped ends. Posiadala [6] used Lagrange multiplier method to analyze a simply supported beam supported by a spring at its span, or simply supported two span beams to which one mass–spring system is added. He got natural frequency parameters and showed them in frequency parameter diagrams. Gürgöze [7] used Lagrange multiplier method for a cantilever beam with tip mass when it has a mass–spring at the free end, or the free end is supported by spring, to obtain natural frequencies.

Das and Navakatna [8] extended Young's study [1] to a simply supported rectangular plate at which one point is supported by a mass–spring system. Snowdon [9] studied forced vibration of a simply supported rectangular plate with an added mass or with a mass–spring–dashpot system, and obtained force transmissibility and driving-point impedance of a plate. Nicholson and Bergman [10] extended their study [8] to a plate system. Trentin and Guyader [11] used modal sampling method to study response of a plate at medium frequency range in which a large number of modes exist. Similar problem for a plate with mass–spring system was analyzed by Dowell and Tang [12] by using asymptotic modal analysis. Cha and Wong [13] presented a method to analyze combined dynamical system and compared the results with those by the Lagrange multiplier method, and the Green function method. In the optimization problem, to maximize the fundamental natural frequency by adding support springs, Won and Park [14] treated cantilever beam and plate.

In these studies, influences of added mass, added spring support, or added spring–mass have been treated. The obtained results, however, are presented in the form of frequency equation, or at most natural frequencies in tables or some graphs, which do not give enough information as engineering design data.

In the present study, we shall treat a cantilever plate attached by a 'spring–mass' system, and systematically clarify the coupled vibration characteristics of the system by thoroughly studying the effects of the 'spring–mass' attachment. Rayleigh–Ritz method is used in the derivation of the frequency equations.

2. Basic equation

We shall consider coupled free vibration of a thin cantilever plate attached by a 'spring–mass' system. Cartesian co-ordinate system x–y is taken as shown in Fig. 1. The plate is thin and isotropic, and has width H, length L, and thickness h. While the 'spring–mass' system has a spring constant k_e and mass m_e, and is attached to (x_0, y_0) on the plate. Displacements of the plate and mass are represented as $W(x, y, t)$ and $z(t)$ respectively. Here, we shall employ the classical plate theory.

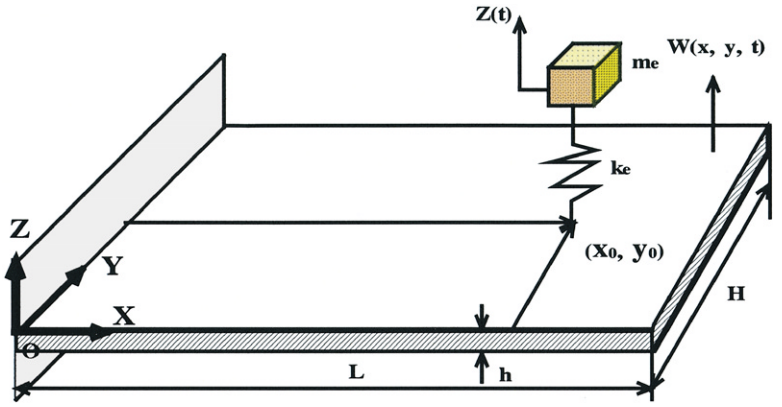

Fig. 1. Cantilever plate with 'spring–mass' system.

For linear free vibration of the coupled system, strain energy U and kinetic energy T are

$$U = \frac{D}{2}\int_0^H \int_0^L \left[\left(\frac{\partial^2 W(x,y,t)}{\partial x^2} + \frac{\partial^2 W(x,y,t)}{\partial y^2} \right)^2 + 2(1-\nu)\left\{ \left(\frac{\partial^2 W(x,y,t)}{\partial x \partial y} \right)^2 - \frac{\partial^2 W(x,y,t)}{\partial x^2}\frac{\partial^2 W(x,y,t)}{\partial y^2} \right\} \right] \mathrm{d}x\,\mathrm{d}y + \frac{1}{2}k_e\{z(t) - W(x_0,y_0,t)\}^2, \tag{1}$$

$$T = \frac{\rho h}{2}\int_0^H \int_0^L \dot{W}^2(x,y,t)\,\mathrm{d}x\,\mathrm{d}y + \tfrac{1}{2}m_e\dot{z}^2(t), \tag{2}$$

where ρ and D are the density and the flexural rigidity of the plate, respectively. We assume that the system vibrates with circular frequency Ω as

$$W(x,y,t) = w(x,y)\mathrm{e}^{\mathrm{i}\Omega t}, \tag{3}$$

$$z(t) = z_0\mathrm{e}^{\mathrm{i}\Omega t}. \tag{4}$$

Then, Eqs. (1) and (2) lead to

$$U_{max} = \frac{D}{2}\int_0^H \int_0^L \left[\left(\frac{\partial^2 w(x,y)}{\partial x^2} + \frac{\partial^2 w(x,y)}{\partial y^2} \right)^2 + 2(1-\nu)\left\{ \left(\frac{\partial^2 w(x,y)}{\partial x \partial y} \right)^2 - \frac{\partial^2 w(x,y)}{\partial x^2}\frac{\partial^2 w(x,y)}{\partial y^2} \right\} \right] \mathrm{d}x\,\mathrm{d}y + \tfrac{1}{2}k_e\{z_0 - w(x_0,y_0)\}^2, \tag{5}$$

$$T_{max} = \Omega^2\left\{ \frac{\rho h}{2}\int_0^H \int_0^L w^2(x,y)\,\mathrm{d}x\,\mathrm{d}y + \tfrac{1}{2}m_e z_0^2 \right\}. \tag{6}$$

The Lagrangian of the system is

$$\tilde{L} = U_{max} - T_{max}$$
$$= \frac{D}{2}\int_0^H \int_0^L \left[\left(\frac{\partial^2 w(x,y)}{\partial x^2} + \frac{\partial^2 w(x,y)}{\partial y^2} \right)^2 + 2(1-\nu)\left\{ \left(\frac{\partial^2 w(x,y)}{\partial x \partial y} \right)^2 - \frac{\partial^2 w(x,y)}{\partial x^2}\frac{\partial^2 w(x,y)}{\partial y^2} \right\} \right] \mathrm{d}x\,\mathrm{d}y$$
$$+ \tfrac{1}{2}k_e\{z_0 - w(x_0,y_0)\}^2 - \Omega^2\left\{ \frac{\rho h}{2}\int_0^H \int_0^L w^2(x,y)\,\mathrm{d}x\,\mathrm{d}y + \tfrac{1}{2}m_e z_0^2 \right\}. \tag{7}$$

Here, we shall introduce non-dimensional parameters

$$\xi = \frac{x}{L}, \quad \eta = \frac{y}{H}, \quad \xi_0 = \frac{x_0}{L}, \quad \eta_0 = \frac{y_0}{H}, \quad \bar{w} = \frac{w}{L}, \quad \zeta = \frac{z_0}{L}, \quad \omega^2 = \left(\frac{\Omega}{\Omega_0} \right)^2, \tag{8}$$

$$\Omega_0 = \sqrt{\frac{D}{\rho h L^4}}, \quad \alpha_{me} = \frac{m_e}{\rho H h L}, \quad \alpha_{ke} = \frac{k_e L^2}{D}, \quad \lambda = \frac{L}{H},$$

where λ is the aspect ratio of the plate, α_{me} and α_{ke} are the mass ratio and the stiffness ratio between the 'spring–mass' system and the plate. Then, Eq. (7) is represented as

$$\tilde{L} = \int_0^1 \int_0^1 \left[\left(\frac{\partial^2 \bar{w}}{\partial \xi^2} \right)^2 + 2\nu\lambda^2 \frac{\partial^2 \bar{w}}{\partial \xi^2}\frac{\partial^2 \bar{w}}{\partial \eta^2} + \lambda^4 \left(\frac{\partial^2 \bar{w}}{\partial \eta^2} \right)^2 + 2(1-\nu)\lambda^2 \left(\frac{\partial^2 \bar{w}}{\partial \xi \partial \eta} \right)^2 \right] \mathrm{d}\xi\,\mathrm{d}\eta$$
$$+ \alpha_{ke}\lambda\{\zeta - \bar{w}(\xi_0,\eta_0)\}^2 - \omega^2\left\{ \int_0^1 \int_0^1 \bar{w}^2(\xi,\eta)\,\mathrm{d}\xi\,\mathrm{d}\eta + \alpha_{me}\zeta^2 \right\}. \tag{9}$$

3. Method of solution

The displacements of the plate and attached mass are assumed to be of the forms

$$\bar{w}(\xi,\eta) = \sum_m \sum_n a_{mn}\Phi_m(\xi)\Psi_n(\eta),$$
$$\zeta = b, \tag{10}$$

where a_{mn} and b are the unknown parameters. $\Phi_m(\xi)$ and $\Psi_n(\eta)$ are the admissible beam functions, which satisfy *clamped–free* boundary conditions and *free–free* conditions, respectively, which are defined as follows:

$$\Phi_m(\xi) = \mu_m(\cosh\alpha_m\xi - \cos\alpha_m\xi) - \nu_m(\sinh\alpha_m\xi - \sin\alpha_m\xi) \quad (m = 1,2,3,\ldots),$$
$$\mu_m = \frac{\cosh\alpha_m + \cos\alpha_m}{\sinh\alpha_m \sin\alpha_m}, \quad \nu_m = \frac{\sinh\alpha_m - \sin\alpha_m}{\sinh\alpha_m \sin\alpha_m}, \tag{11}$$

where α_m are the roots of

$$\cosh\alpha_m \cos\alpha_m = -1, \tag{12}$$

$\alpha_1 = 1.875$, $\alpha_2 = 4.694$, $\alpha_3 = 7.854$, … for *clamped–free* beam function;

$$\Psi_1(\eta) = 1,$$

$$\Psi_2(\eta) = \sqrt{3}(2\eta - 1),$$

$$\Psi_n(\eta) = \bar{\mu}_n(\cosh\beta_n\eta + \cos\beta_n\eta) - \bar{\nu}_n(\sinh\beta_n\eta + \sin\beta_n\eta) \quad (n = 3, 4, 5, \ldots), \tag{13}$$

$$\bar{\mu}_n = \frac{\cosh\beta_n - \cos\beta_n}{\sinh\beta_n \sin\beta_n}, \quad \bar{\nu}_n = \frac{\sinh\beta_n + \sin\beta_n}{\sinh\beta_n \sin\beta_n},$$

where β_n $(3 \leqslant n)$ are the roots of

$$\cosh\beta_n \cos\beta_n = 1, \tag{14}$$

$\beta_3 = 4.730$, $\beta_4 = 7.853$, $\beta_5 = 10.995$, … for *free–free* beam function.

Substituting Eq. (10) into Eq. (9), and applying Rayleigh–Ritz method, we can derive the natural frequency equation in a matrix form as

$$\left[\begin{pmatrix} \dfrac{\alpha_{ke}}{\alpha_{me}}\lambda & -\dfrac{\alpha_{ke}}{\alpha_{me}}\lambda\Phi_r(\xi_0)\Psi_s(\eta_0) \\ -\alpha_{ke}\lambda\Phi_m(\xi_0)\Psi_n(\eta_0) & K_{mnrs} + \alpha_{ke}\lambda\Phi_m(\xi_0)\Psi_n(\eta_0)\Phi_r(\xi_0)\Psi_s(\eta_0) \end{pmatrix} - \omega^2 \begin{pmatrix} 1 & 0 \\ 0 & \delta_{mr}\delta_{ns} \end{pmatrix}\right] \begin{Bmatrix} b \\ a_{rs} \end{Bmatrix} = \mathbf{0}, \tag{15}$$

$$K_{mnrs} = (\alpha_m^4 + \lambda^4\beta_n^4)\delta_{mr}\delta_{ns} + \nu\lambda^2(J_{mr}^{20}K_{ns}^{02} + J_{mr}^{02}K_{ns}^{20}) + 2(1-\nu)\lambda^2 J_{mr}^{11}K_{ns}^{11} \tag{16}$$

and

$$[\mathbf{K} - \omega^2\mathbf{M}]\begin{Bmatrix} b \\ a_{rs} \end{Bmatrix} = \mathbf{0}, \tag{17}$$

$$\mathbf{K} = \begin{bmatrix} \dfrac{\alpha_{ke}}{\alpha_{me}}\lambda & -\dfrac{\alpha_{ke}}{\alpha_{me}}\lambda\Phi_r(\xi_0)\Psi_s(\eta_0) \\ -\alpha_{ke}\lambda\Phi_m(\xi_0)\Psi_n(\eta_0) & K_{mnrs} + \alpha_{ke}\lambda\Phi_m(\xi_0)\Psi_n(\eta_0)\Phi_r(\xi_0)\Psi_s(\eta_0) \end{bmatrix}, \tag{18}$$

$$\mathbf{M} = \begin{bmatrix} 1 & 0 \\ 0 & \delta_{mr}\delta_{ns} \end{bmatrix}, \quad m = 1, 2, \ldots, \quad n = 1, 2, , \ldots, \quad r = 1, 2, , \ldots, m, \quad s = 1, 2, \ldots, n, \tag{19}$$

from which one can get coupled natural frequencies as eigenvalues, and vibration modes as eigenvectors. $\boldsymbol{K}$ and $\boldsymbol{M}$ are square matrices with size $(1 + m \times n) \times (1 + m \times n)$. Details of the derivation of Eq. (15) are in Appendix B.

4. Numerical results

The present plate – 'spring–mass' coupled dynamical system can be represented by four system parameters: aspect ratio of a plate $\lambda \equiv L/H$, stiffness ratio $\alpha_{ke} \equiv k_e L^2/D$, mass ratio $\alpha_{me} \equiv m_e/\rho HhL$, and attached position of a 'spring–mass' system (ξ_0, η_0). Numerical calculations have been carried out varying these system parameters to clarify the influence of attached 'spring–mass' system on the coupled dynamical characteristics of a plate. The Poisson ratio ν was taken as 0.3. In the calculation, unknown terms in Eq. (15) were taken up to $m = n = r = s = 7$, to get reliable values as engineering data.

4.1. Uncoupled vibrations of plate and 'spring–mass' system

First, we shall see the uncoupled vibration characteristics of a plate and a 'spring–mass' system respectively. Variations of uncoupled natural frequencies of a cantilever plate ω_0 with aspect ratio λ are shown in Fig. 2. For convenience, vibration modes when $\lambda = 4.0$ are presented in the right-hand side of the figure. In general, natural frequencies that have nodal line in vibration mode perpendicular to the plate axis (ξ) are nearly constant with λ, while those which have nodal line parallel to the plate axis increase with increase in λ. With the variation of λ, mode exchange can be observed. Furthermore, one can recognize the veering and crossing of the frequency curves [15, 16]. In order to distinguish these two, step size for λ in the numerical calculation was taken to be small as much as possible. More details on frequency curve's veering and crossing in a cantilever

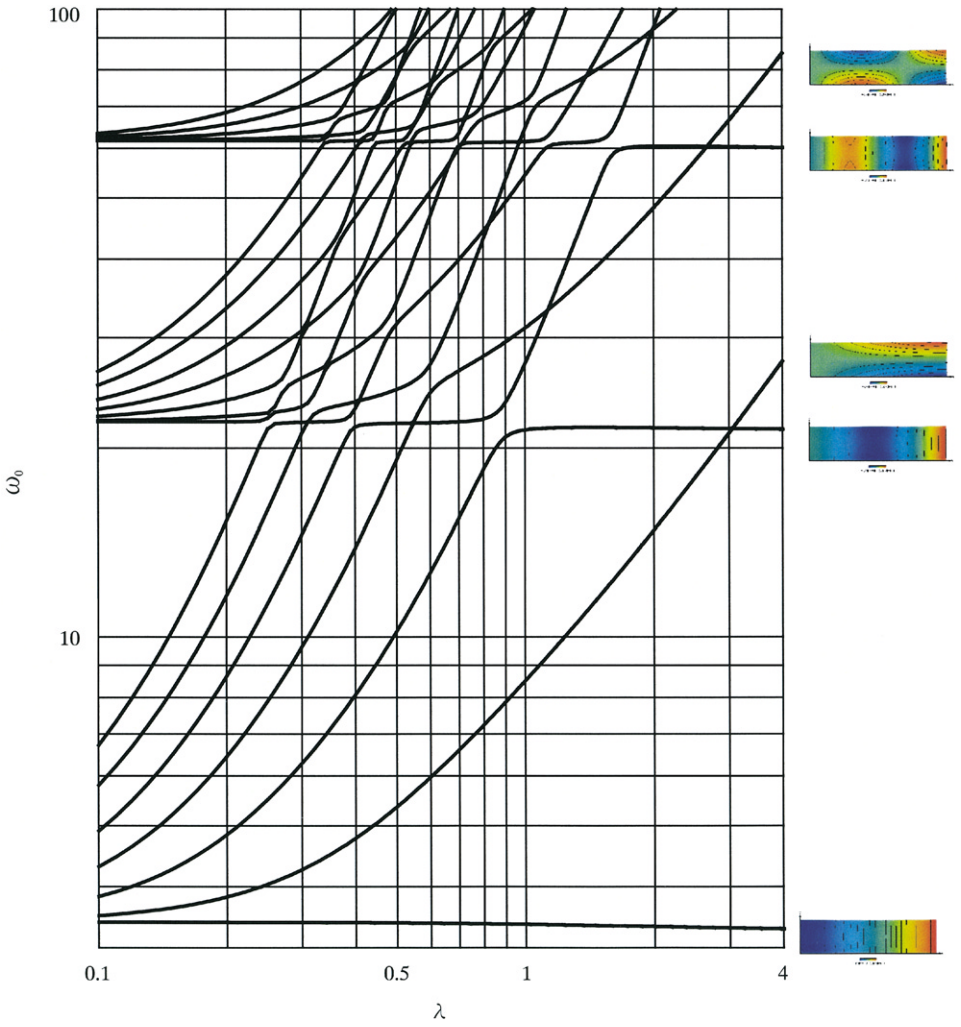

Fig. 2. Uncoupled natural frequency of a plate with aspect ratio λ.

plate have been studied in Ref. [17]. In Fig. 3, the lowest five vibration modes are presented for three kinds of aspect ratio $\lambda = 0.5$, 1 and 2, which show mode change with λ.

Uncoupled natural frequency variations of the 'spring–mass' system alone with mass ratio α_{me} are presented in Fig. 4, for stiffness ratio $\alpha_{ke} = 0.1$, 1, 10, 100, and $\lambda = 1$, 2, 3. In this case, uncoupled natural frequency of the 'spring–mass' system is given by $\omega_{sp} = \sqrt{\alpha_{ke}\lambda/\alpha_{me}}$ from Eq. (15). It decreases with increase in the mass ratio α_{me} and increases with increase in the stiffness ratio α_{ke}. In the figures shown hereafter, uncoupled natural frequency of the 'spring–mass' system is represented by dashed line, for reference.

4.2. Coupled system

4.2.1. Influences of α_{ke} and α_{me}

For a square plate with $\lambda = 1.0$, coupled natural frequency $\omega - \alpha_{me}$ diagrams have been obtained, changing the attached position of the 'spring–mass' system as $(\xi_0, \eta_0) = (0.5, 0.3)$, (1.0, 1.0), (0.5, 0.5), (1.0, 0.5) as shown in Fig. 5. In Fig. 6, as one of the examples, the results for $(\xi_0, \eta_0) = (0.5, 0.5)$, i.e., the 'spring–mass' system is attached on the middle of the plate, are presented when $\alpha_{ke} = 0.1$, 1, 10, 100. In the figures, one dotted line corresponds to the uncoupled natural frequencies of a plate without 'spring–mass' system, ω_o: there exist four uncoupled natural frequencies below $\omega = 30$. Dashed curve corresponds to the natural frequency of an uncoupled 'spring–mass' system ω_{sp}, which depends on both α_{ke} and α_{me} as shown in Fig. 4. This curve appears in the diagram for lower α_{me} region below the first mode of the plate when $\alpha_{ke} = 0.1$: Fig. 6(a), in this case, it is nearly coincident with a coupled natural frequency curve. With increase in α_{ke}, uncoupled natural frequency ω_{sp} increases and the number of the interactions with uncoupled plate frequency lines increase, in which strong couplings are expected in these regions.

Dowell [3] noted in his paper on dynamical coupling of a beam with spring–mass system, that 'if a spring–mass oscillator is attached to another system, a new natural frequency appears between the original pair of frequencies nearest to the oscillator natural frequency'. In the present system, although the treating system is not the same, the same conclusion can be obtained, as will be illustrated in Fig. 6.

Then, we shall see the influence of the stiffness ratio α_{ke} ($\equiv k_e L^2/D$). When α_{ke} is small as 0.1 (Fig. 6(a)), i.e., the stiffness of the attached 'spring–mass' system is relatively smaller than that of a plate, the lowest coupled natural frequency corresponds to the vibration mode in which the motion of the 'spring–mass' system is predominant. And the higher modes correspond to those in which plate motion is predominant. This means that the coupling is weak, in these cases.

With increase of α_{ke} to 1 (Fig. 6(b)), coupling between the plate and the 'spring–mass' system can be recognized at the regions $\alpha_{me} = 0.01$ and 0.1, i.e., with the first and the second plate modes; while in the other regions in the graph, there seems no influence of the attached 'spring–mass' system. As variations of frequency curve with α_{me}, one can see that the frequency curve of a plate is forced to bend or is strongly influenced by that of the 'spring–mass' system.

On further increase in α_{ke} to 10 (Fig. 6(c)), the coupling regions become wide, i.e., with the first, second, third and fourth plate modes. It is to be noted here that as α_{me} increases, the natural frequency curve of the first plate mode tends to that of the uncoupled 'spring–mass' system. While natural frequency curve for the second plate mode tends to that of the first plate mode, but the value is a little higher than that of the first uncoupled plate mode. Similarly, natural frequency

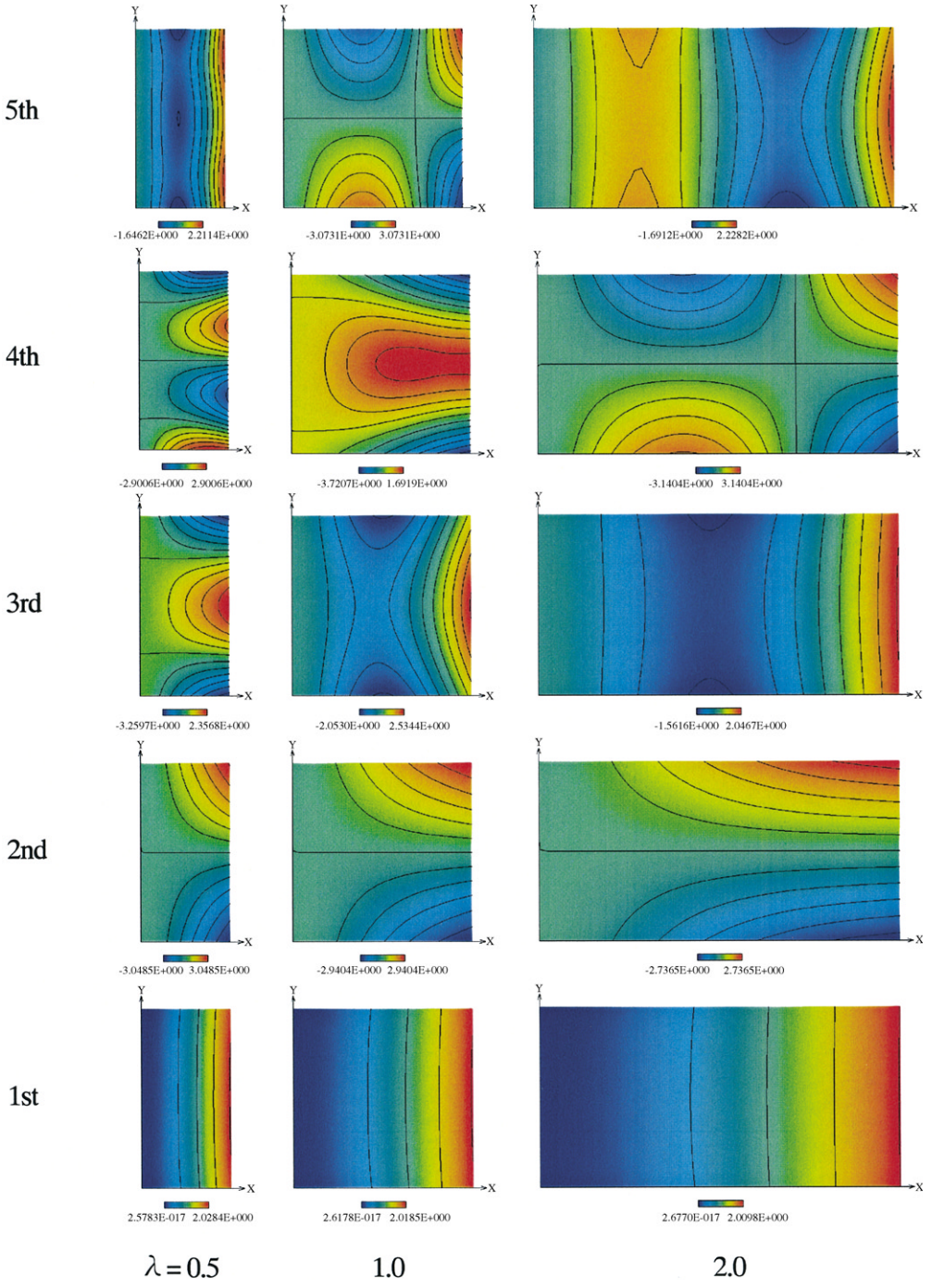

Fig. 3. Vibration mode variation of a cantilever plate with aspect ratio λ : $\lambda = 0.5$, 1, 2.

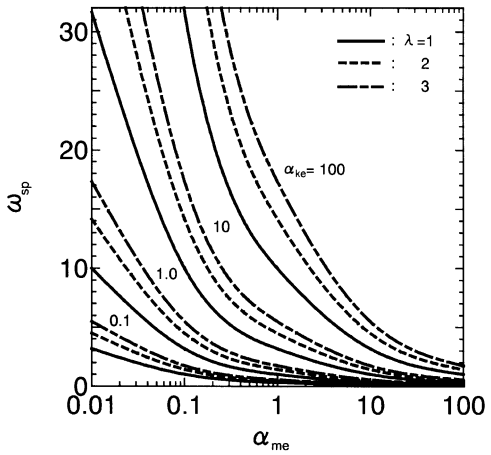

Fig. 4. Uncoupled natural frequency of a 'spring–mass' system: $\lambda = 1, 2, 3$, $\alpha_{ke} = 0.1, 1, 10, 100$.

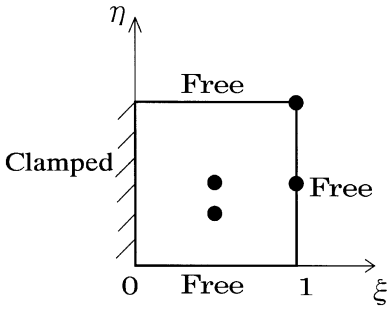

Fig. 5. Attached position (ξ_0, η_0) of a 'spring–mass' system on the plate.

curve for the third plate mode tends to that of the second plate modes. Such variations can be seen more clearly when $\alpha_{ke} = 100$, Fig. 6(d).

To understand these phenomena from another point of view, we then see the influence of the attached 'spring–mass' system on the vibration mode, instead of just concentrating on at the frequency curve variation. As an example, vibration modes are shown in Fig. 7(a) as contour diagrams, and in Fig. 7(b) as cross-sectional diagrams along the center axis of a plate ($\eta = 0.5$) when $\alpha_{ke} = 10$, which corresponds to Fig. 6(c). In these figures, the maximum displacement of the plate or attached mass is normalized to unity, and we use the order of vibration mode according to the order of the frequency magnitude, i.e., the first, second … .

Let us look at the results when $\alpha_{me} = 0.01$, i.e., the first column of Fig. 7(a) and (b), and the left-hand side of Fig. 6(c). In this case, mass ratio α_{me} ($\equiv m_e/\rho HhL$) is small, i.e., attached mass is relatively smaller than that of the plate, the displacement of the attached mass is same as that of the plate at the first, second and fifth modes, except third and fourth modes in which the influence of 'spring–mass' system is significant. Here, we have to note that in the second and fifth modes,

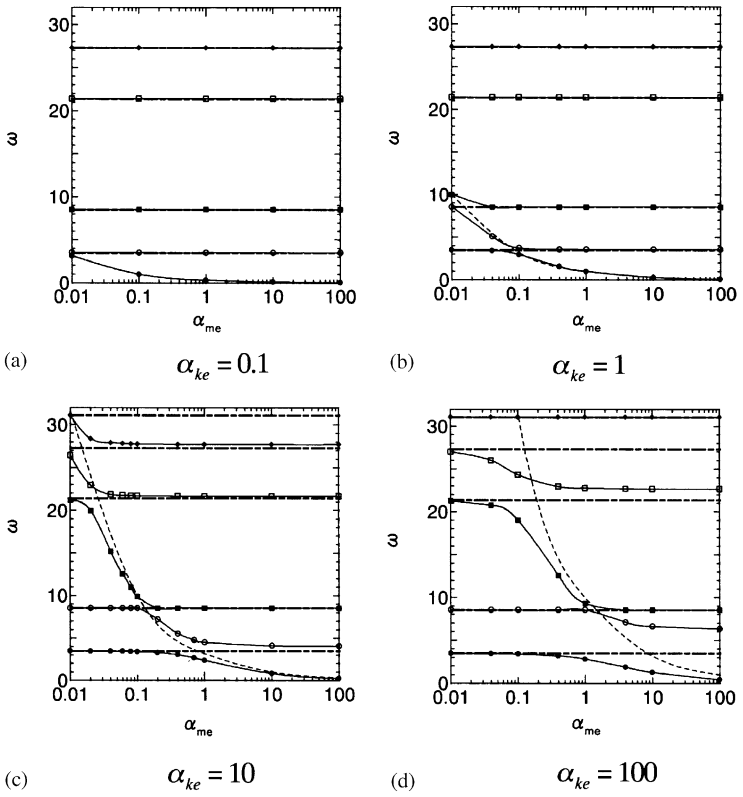

Fig. 6. Variation of coupled natural frequencies with α_{me}: - · - · - · -, ω_o; - - - - -, ω_{sp}; $\lambda = 1$, $(\xi_0, \eta_0) = (0.5, 0.5)$, $\alpha_{ke} = 0.1$, 1, 10, 100.

the 'spring–mass' system is attached just on the vibration mode, so that the coupling may be very weak.

With increase in α_{me}, the lowest coupled vibration mode, i.e., the first mode, changes from the first plate mode to the 'spring–mass' system predominant mode, while the second mode changes from the second plate mode to the first plate mode. As mentioned previously, natural frequencies of the second vibration mode with large $\alpha_{me}(= 1, 10, 100)$ are a little higher than that of the uncoupled plate. This can be clearly explained by looking at Fig. 7(b), i.e., the displacements of the plate and mass are not the same which makes the spring's elongation increase the natural frequency in these modes. This is also true for the fourth mode.

4.2.2. Influence of attached position (ξ_0, η_0) of a 'spring–mass' system

To consider the influence of the attached position of a 'spring–mass' system, the results when the 'spring–mass' system is attached to the other position $(\xi_0, \eta_0) = (1.0, 1.0)$, i.e. the 'spring–mass' system is attached to the free end corner of a plate, are presented in Figs. 8 and 9. Adding the 'spring–mass' system out of the centerline of the plate width, vibration mode becomes asymmetric as shown in Fig. 9(a), i.e., the nodal line parallel to ξ axis is shifted to the attached direction of the

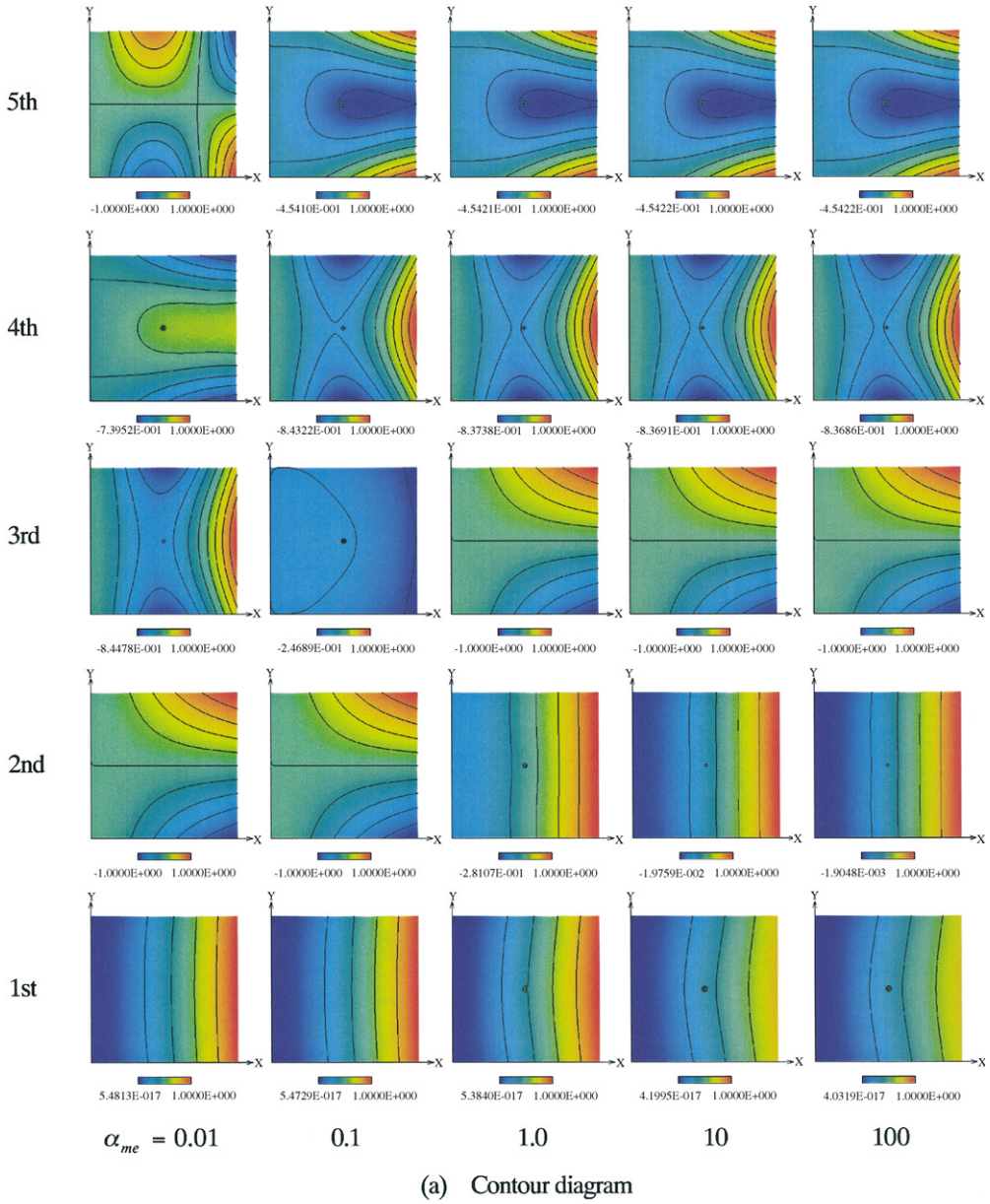

Fig. 7. Variation of vibration mode with α_{me}, $\lambda = 1$, $\alpha_{ke} = 10$, $(\xi_0, \eta_0) = (0.5, 0.5)$: (a) contour diagram; (b) sectional mode along $\eta_0 = 0.5$.

system on the plate. Furthermore, the natural frequencies of the second, third and fifth modes become higher than those of the uncoupled ones in the range $\alpha_{me} = 0.1 \sim 100$, because of the restriction of the plate displacement where maximum displacement occurs, i.e., free end of the plate, which makes the maximum displacement at the opposite end corner of the plate.

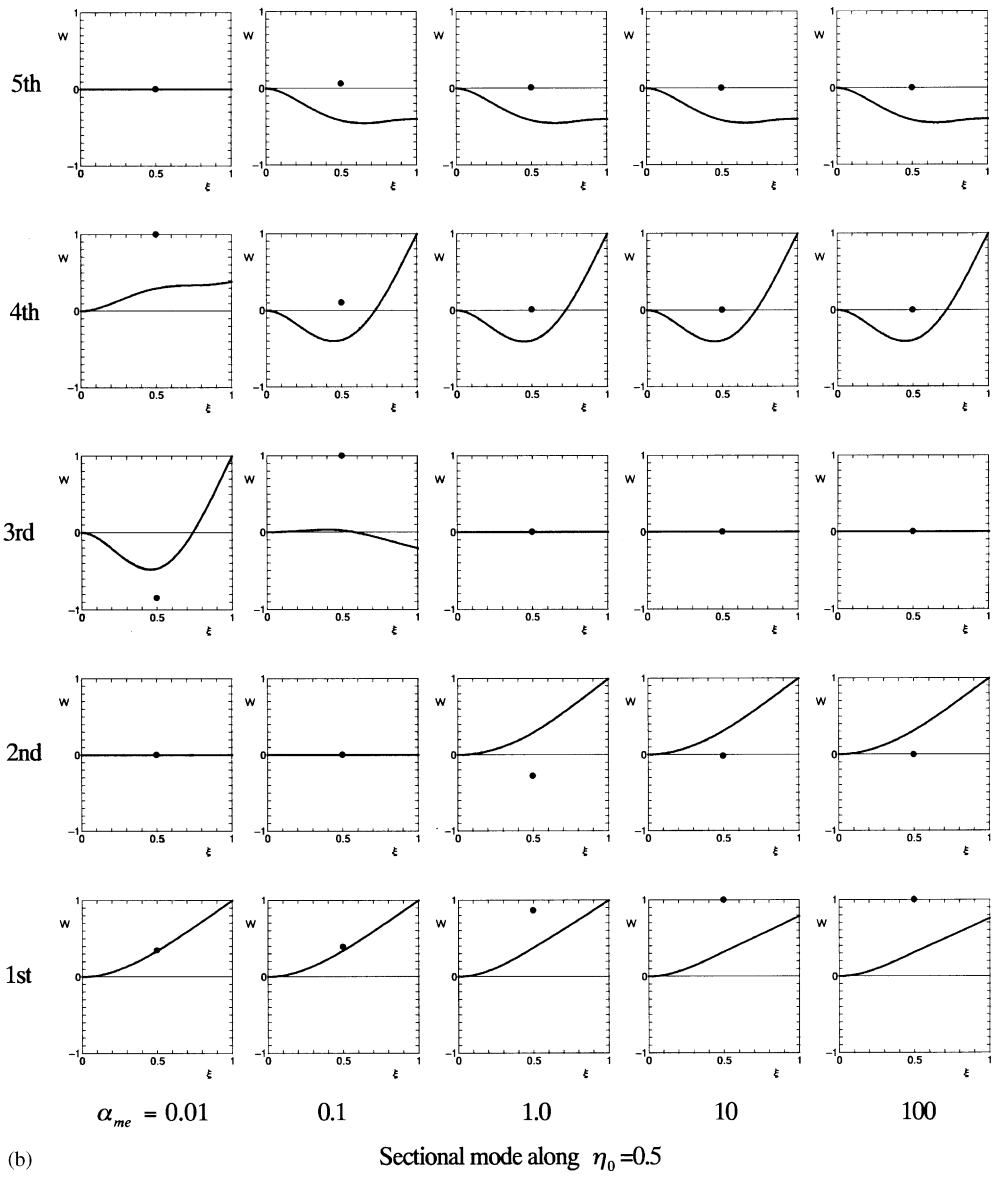

Fig. 7 (*continued*).

We cannot present all the calculated results for other attached positions for the limited space. The influence of the attached 'spring–mass' system can summarized as follows:

1. When the attached position coincides with the vibration node of a plate at its *j*th normal mode, there is no movement of the attached mass, which makes no change in the plate *j*th natural frequency.

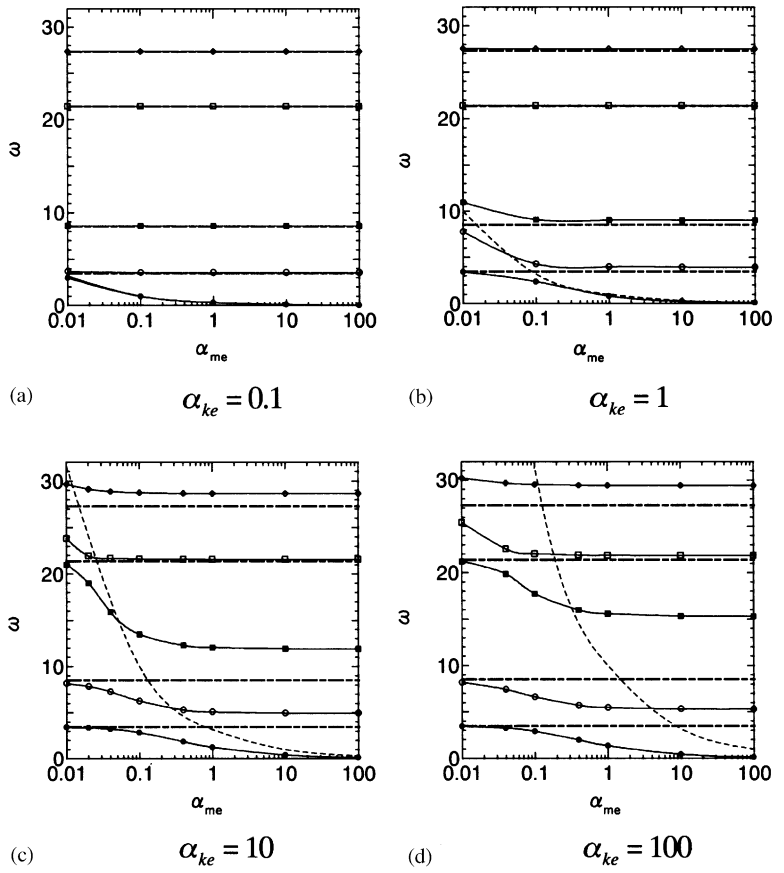

Fig. 8. Variation of coupled natural frequencies with α_{me}; - · - · - · -, ω_o; - - - - -, ω_{sp}; $\lambda = 1$, $(\xi_0, \eta_0) = (1.0, 1.0)$, $\alpha_{ke} = 0.1$, 1, 10, 100.

2. With increase in α_{ke} and α_{me}, movement of the plate is constrained by the attached system that decreases the displacement of plate at that point and increases the coupled natural frequency.
3. When the stiffness ratio α_{ke} is as small as 0.1, the influence of the attached system at any point on a plate is small, independent of the α_{me} value.

4.2.3. Maximizing natural frequencies

In the previous section, coupled vibration characteristics have been investigated for the plate with $\lambda = 1$, showing the frequency diagrams and the vibration modes. In this section, we shall focus on the effect of the attached 'spring–mass' system on the natural frequency of a cantilever plate.

At the beginning, we treat here again a plate with $\lambda = 1$ and the lowest three vibration modes shown in Fig. 3. Changing the parameters α_{ke} and α_{me} as 1, 10, 100 and attached position (ξ_0, η_0) of the 'spring–mass' system, natural frequencies have been calculated and are shown in Fig. 10. In each diagram, the position η_0 is presented in the abscissa, while the natural frequency ratio ω/ω_0 normalized by that of a plate without attached system ω_0 is shown in the ordinate. And 'Mode 1',

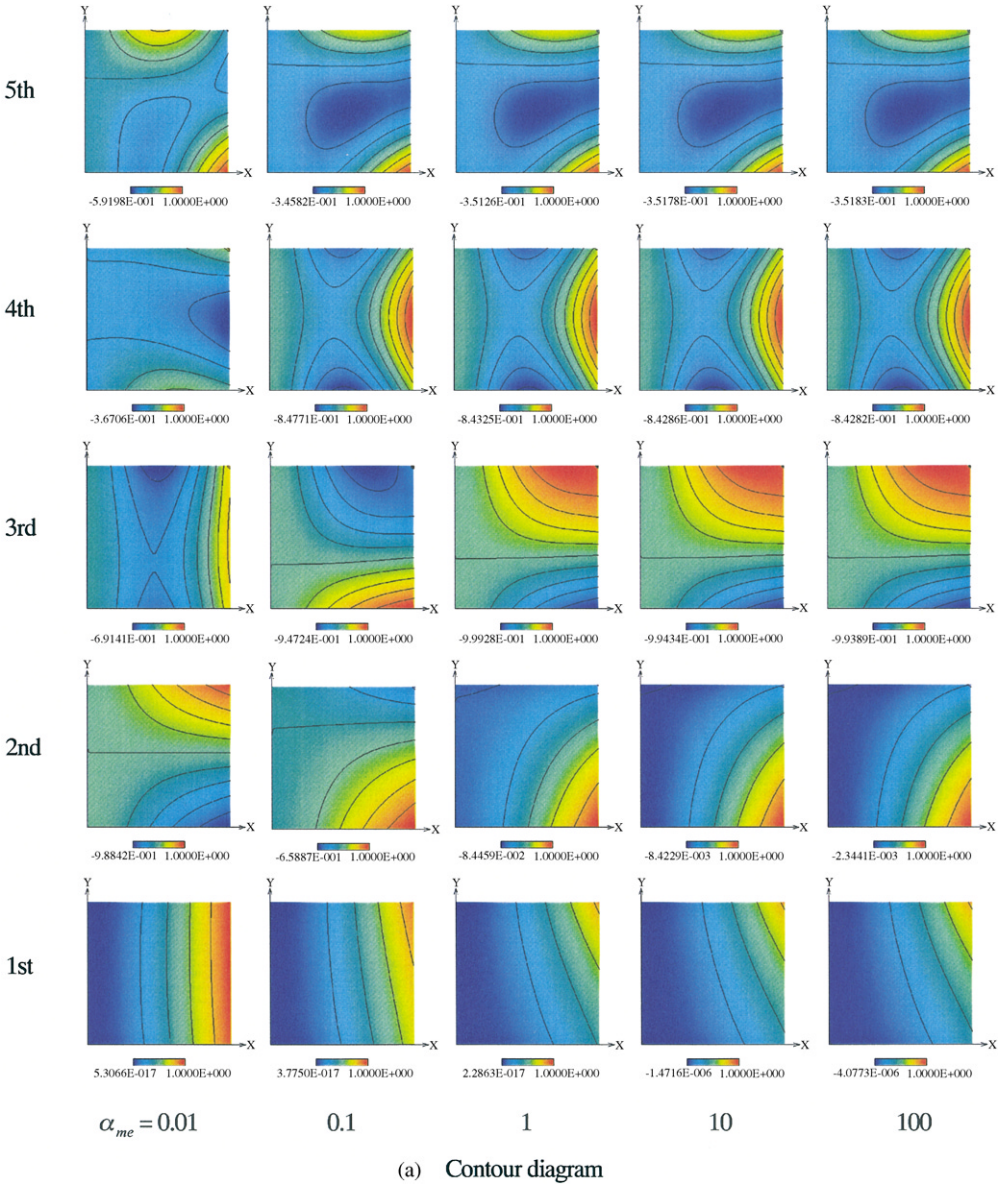

Fig. 9. Variation of vibration mode with α_{me}, $\lambda = 1$, $\alpha_{ke} = 10$, $(\xi_0, \eta_0) = (1.0, 1.0)$: (a) contour diagram; (b) sectional mode along $\eta_0 = 1.0$.

'Mode 2', and 'Mode 3' correspond to the lowest three vibration modes shown in Fig. 3 when $\lambda = 1$.

We will see first Mode 1 which are shown in the lowest diagram in Fig. 10, and when $\alpha_{ke} = \alpha_{me} = 1$. Although the influence of the attached system on the vicinity of a clamped end as $\xi_0 = 0.2$ and 0.4 is small, that on the free end of the plate, i.e., $\xi_0 = 1.0$, is significant which increases the natural frequency. Curve when $\xi_0 = 0.2$ for $\alpha_{ke} = \alpha_{me} = 1$ nearly coincides with the

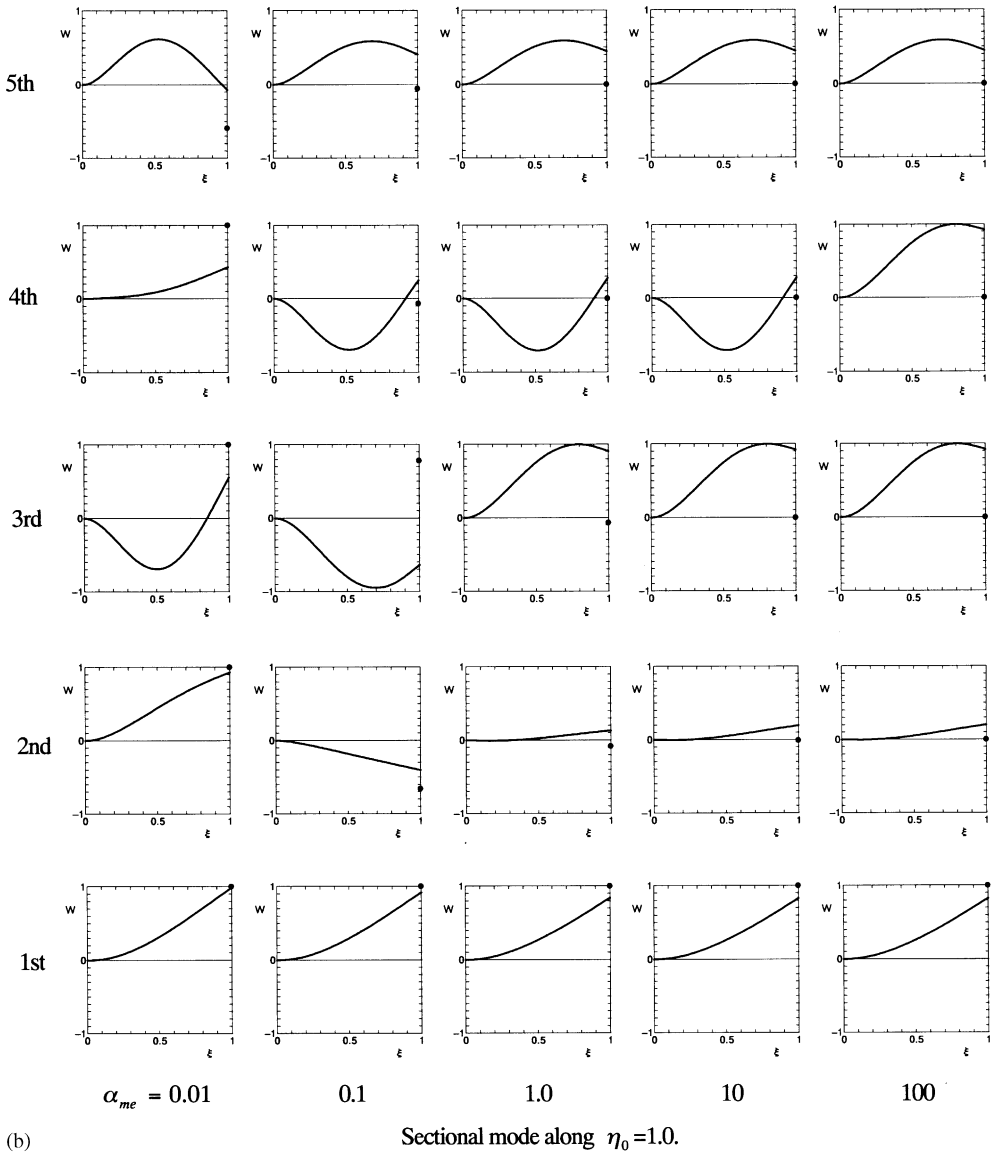

Fig. 9 (*continued*).

η_0 axis. Consequently, the maximum natural frequency ratio of factor 1.16 is obtained when $(\xi_0, \eta_0) = (1.0, 0.5)$, i.e., when the 'spring–mass' system is attached to the middle free end of the plate. The reason why the maximum cannot be obtained at the position $(\xi_0, \eta_0) = (1.0, 0)$ or (1.0, 1.0), i.e., at the free end corners, may be considered because the displacement of the other free end corner becomes large when the 'spring–mass' system attaches to one of the free end corners, as shown in Fig. 9(a), which has a lower natural frequency than that of the mode when the corner is constrained. With an increase of α_{ke} and α_{me}, shown in Fig. 10(b) and (c), the factor of the frequency ratio increases, for example up to 2.5 when $\alpha_{ke} = \alpha_{me} = 100$. In order to grasp these

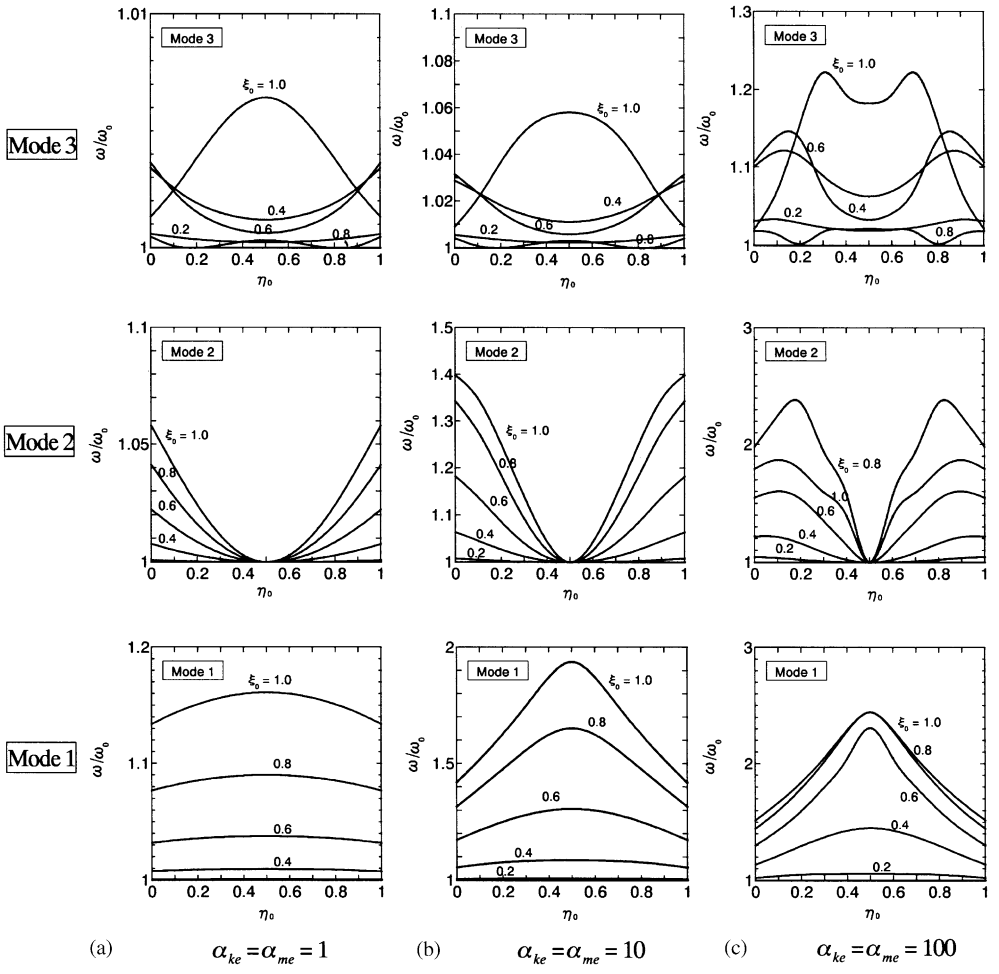

Fig. 10. Frequency ratio $\omega/\omega_0$with attached position (ξ_0, η_0), $\lambda = 1$: (a) $\alpha_{ke} = \alpha_{me} = 1$; (b) $\alpha_{ke} = \alpha_{me} = 10$; (c) $\alpha_{ke} = \alpha_{me} = 100$.

more clearly, the above results are represented in two-dimensional contour diagrams in Fig. 11, from which we can see the above visually.

Next, we will see Mode 2. In this case, since the vibration mode has a nodal line in the middle of the plate, i.e., $\eta_0 = 0.5$, there is no influence of the attached system on the nodal line ($\eta_0 = 0.5$). The effect becomes stronger as the attached position moves to the free end side from the nodal line, or as it moves to the free end from the clamped side. And the maximum occurs at the free end corner of the plate. However, with increase of α_{ke} and α_{me}, this point moves away from the free end corner to the interior region of the plate as shown in Fig. 11(c), which is due to the change of the vibration mode according to the increase of α_{ke} and α_{me}.

As for Mode 3, the frequency ratio locally takes its maximum when the added system is either on the middle end side of the plate $\eta_0 = 0.5$ or on the middle of the free end when $\alpha_{ke} = \alpha_{me} = 1$

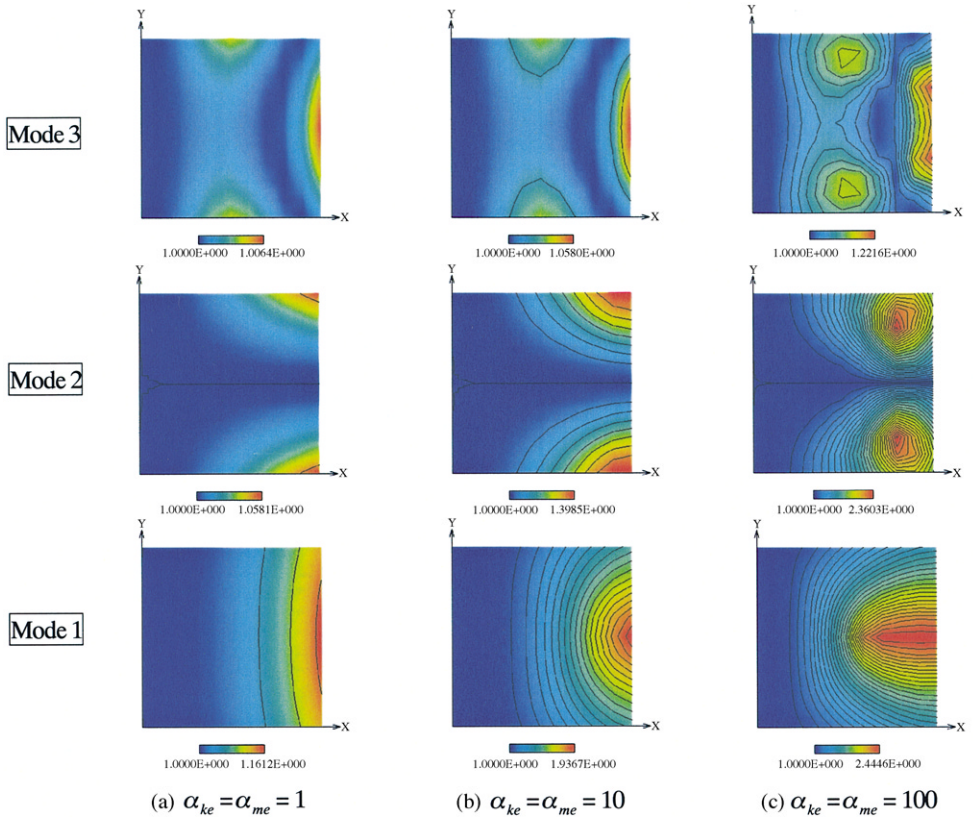

Fig. 11. Frequency ratio ω/ω_0 with attached position (ξ_0, η_0), $\lambda = 1$: (a) $\alpha_{ke} = \alpha_{me} = 1$; (b) $\alpha_{ke} = \alpha_{me} = 10$; (c) $\alpha_{ke} = \alpha_{me} = 100$.

and 10, and the former moves to $\xi_0 = 0.4$ or 0.6 when $\alpha_{ke} = \alpha_{me} = 100$, from which we can see that this mode has vibration characteristics of both Mode 1 and Mode 2.

Here, it should be noted that we put α_{ke} and α_{me} values to be equal, and changed their values, but α_{ke} is the predominant parameter in this characteristic. As an example, similar results when keeping $\alpha_{ke} = 1.0$ and varying α_{me} as 1, 10, 100 are shown in Fig. 12, in which there seems no influence of α_{me}.

4.2.4. *Influence of aspect ratio* λ

So far, we have considered a square plate with $\lambda = 1.0$. Now, we shall examine the effect of aspect ratio λ on the coupled natural frequency ratio. In Fig. 13, the results are presented for $\lambda = 0.5, 1, 2, 3$, when $\alpha_{ke} = \alpha_{me} = 1$: (a) and $\alpha_{ke} = \alpha_{me} = 100$: (b). For Mode 1, the attached point which makes the plate to have the maximum frequency ratio is the middle free end, independent of λ when $\alpha_{ke} = \alpha_{me} = 1$, while this point moves inward the plate on a centerline when $\alpha_{ke} = \alpha_{me} = 100$.

As for Mode 2, this point moves from the free end corner to the clamped side along the free side edge with increase in λ, when $\alpha_{ke} = \alpha_{me} = 1$ and 100.

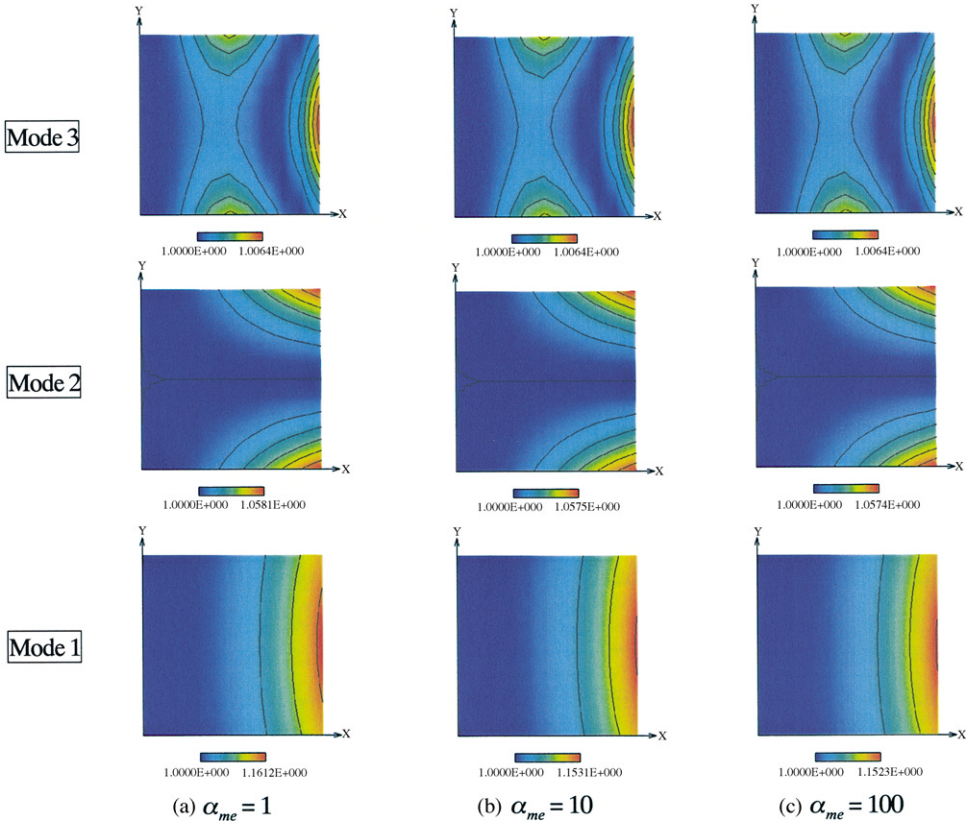

Fig. 12. Influence of α_{me} on frequency ratio ω/ω_0, $\lambda = 1$, $\alpha_{ke} = 1$.

4.2.5. *Plate with attached mass*

In the present study, we can reduce the 'spring–mass' added system to a plate with only 'mass' added system by letting $\alpha_{ke} \to \infty$. In Fig. 14, the coupled natural frequency variations with α_{me} are presented when $(\xi_0, \eta_0) = (0.5, 0.5)$ for $\alpha_{ke} = 10$, 100, 200, 10^3, 10^5. From the figure, we found that with increase in α_{ke}, the natural frequency curves shift to the right-up direction in the diagram and tends to solid lines which correspond to $\alpha_{ke} = 10^5$. In the figure, the horizontal dot-dashed lines correspond to the uncoupled natural frequency without added mass, ω_0. One can see that the natural frequencies for the first, third, fourth modes, except the second and fifth modes, monotonically decrease with increase of α_{me}. The reason why the second and fifth modes remain constant with α_{me} is that the added position $(\xi_0, \eta_0) = (0.5, 0.5)$ just corresponds to the nodal line. As an example of the vibration modes when only 'mass' is added on a square plate are shown in Fig. 15(a): $\alpha_{me} = 0.01$, and in Fig. 15(b): $\alpha_{me} = 10$, when $(\xi_0, \eta_0) = (1.0, 1.0)$ and $\alpha_{ke} = 10^{10}$. Comparing with the results of the 'spring–mass' added system in Fig. 9, coupled vibration modes in which displacement of the 'spring–mass' system is predominant disappeared, and the *mass* and *plate* undergo the same motion at the attached position. Increasing α_{me} (Fig. 15(b)), displacement of the plate is reduced at the mass attached position and this point becomes the nodal point of vibration.

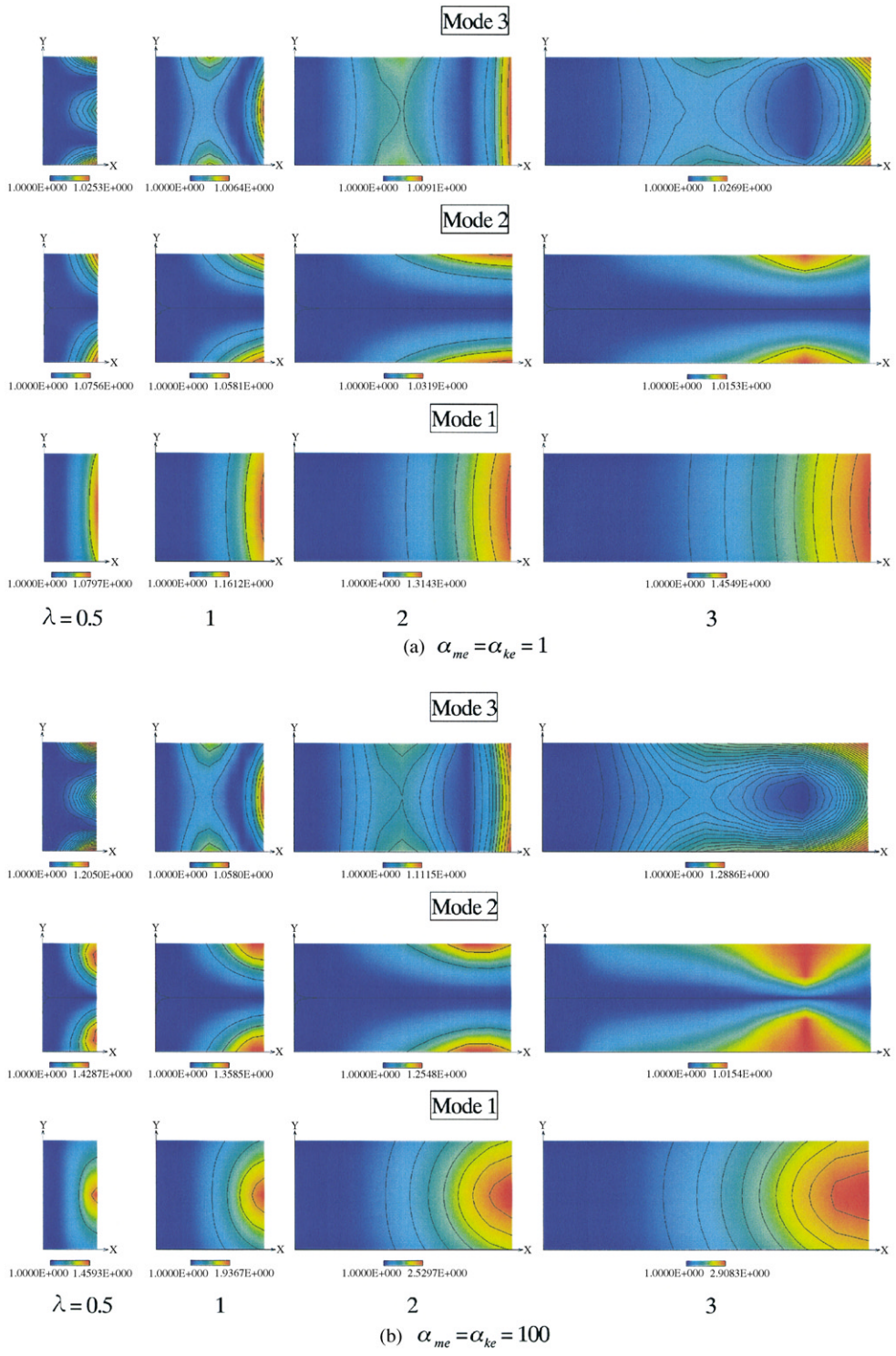

Fig. 13. Influence of aspect ratio λ on frequency ratio ω/ω_0: (a) $\alpha_{ke} = \alpha_{me} = 1$; (b) $\alpha_{ke} = \alpha_{me} = 100$.

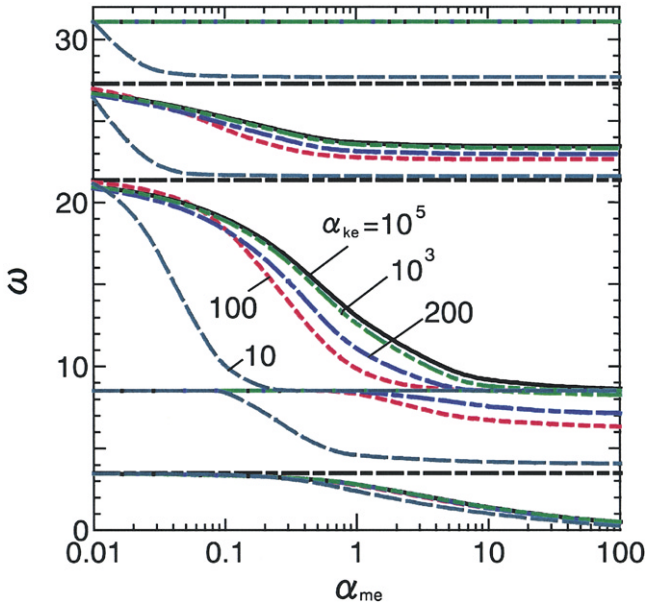

Fig. 14. Variation of natural frequency for only 'mass' attached system with α_{me} for $\alpha_{ke} = 10$, 100, 200, 10^3, 10^5, $(\xi_0, \eta_0) = (0.5, 0.5)$.

Next, we shall examine the natural frequency variations with the 'added mass'. Calculations have been carried out for $\lambda = 0.5$, 1, 2, $\alpha_{me} = 0.01$, 0.1, 1, 10, 100, and $\alpha_{ke} = 10^{10}$. Contrary to the 'spring–mass' added system, the natural frequency of the plate only decreases with the 'added mass', and we will examine the minimum natural frequency here. In Fig. 16, the minimum natural frequency ratio ω_{min}/ω_0 with α_{me} are shown for Mode 1: (a) and Mode 2: (b), and it decreases with increase in α_{me} and the effect of the aspect ratio of the plate λ is different for both Modes 1 and 2. Contour diagrams of the natural frequency ratio for the Modes 1 and 2 are presented in Fig. 17, when $\lambda = 1.0$. When $\alpha_{me} = 0.01$, the minimum natural frequency can be obtained when the mass is attached to the free end side of the plate for Mode 1, and to the free end corner for Mode 2. With increase in α_{me} this point moves inward the clamped direction along the free end sides for Mode 2. For a plate with a different aspect ratio, similar results have been obtained.

So far, we got the coupled natural frequency of the plate which is either higher or lower than the uncoupled one when the 'spring–mass' system is added on the plate. However, we get only the lower coupled natural frequency when only the 'mass' is attached to. Now, we have to consider the difference of the two cases. Let us see, for example, Fig. 18 which is the result when $(\xi_0, \eta_0) = (0.5, 0.5)$, $\alpha_{ke} = 10$. If one chooses the system parameters α_{ke} and α_{me} in the *right*-hand side region of the uncoupled frequency curve of the 'spring–mass' system ω_{sp} or in the larger region than this curve, and increases α_{me}, the coupled natural frequency decreases exchanging vibration mode with that of the 'spring–mass' system, and becomes higher than that of the uncoupled one. While if one chooses the system parameters in the *left*-hand side of the uncoupled frequency curve, there exist no mode exchange and the coupled plate frequency decreases with

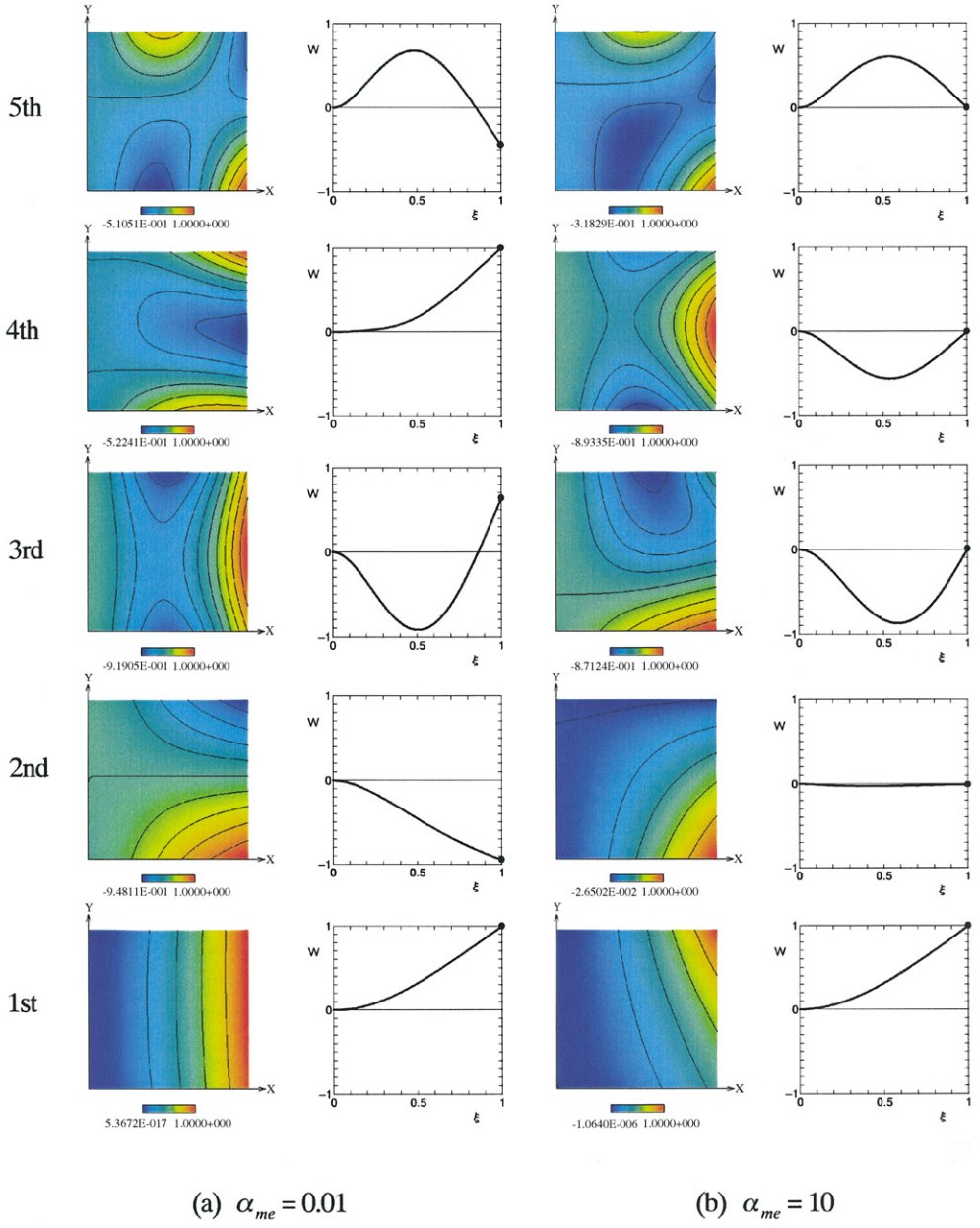

Fig. 15. Vibration mode for 'mass' attached system, $(\xi_0, \eta_0) = (1.0, 1.0)$, $\lambda = 1$, $\alpha_{ke} = 10^{10}$: (a) $\alpha_{me} = 0.01$; (b) $\alpha_{me} = 10$.

increase in α_{me}. Then, if we put $\alpha_{ke} \to \infty$ and get rid of the spring effect, uncoupled frequency curve of the 'spring–mass' system moves to the right-up region in the $\omega - \alpha_{me}$ diagram, so that the left-hand side region becomes relatively wider, in which the natural frequency only decreases.

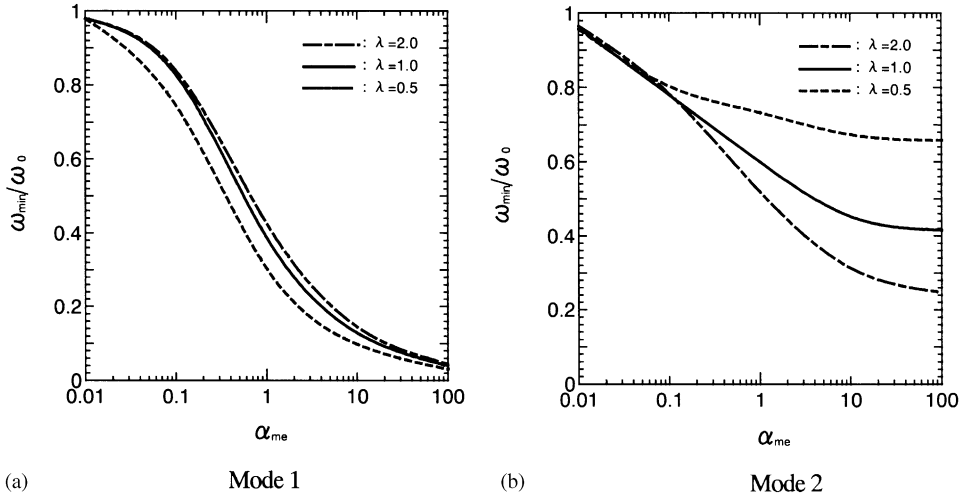

Fig. 16. Minimum natural frequency with α_{me}, $\lambda = 0.5$, 1, 2: (a) Mode 1; (b) Mode 2.

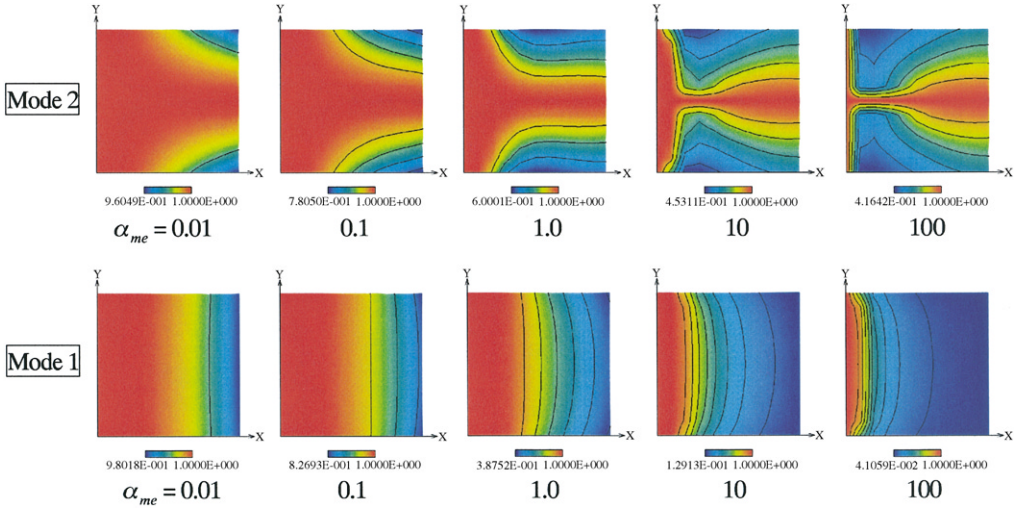

Fig. 17. Influence of α_{me} on frequency ratio of 'mass' attached system, $\alpha_{ke} = 10^{10}$, $\lambda = 1$.

5. Conclusions

The coupled free vibration analysis has been performed on a thin cantilever plate carrying a 'spring–mass' system on an arbitrary point by using Rayleigh–Ritz method. Influence of the attached 'spring–mass' system, i.e., attached position (ξ_0, η_0), stiffness parameter α_{ke}, mass ratio

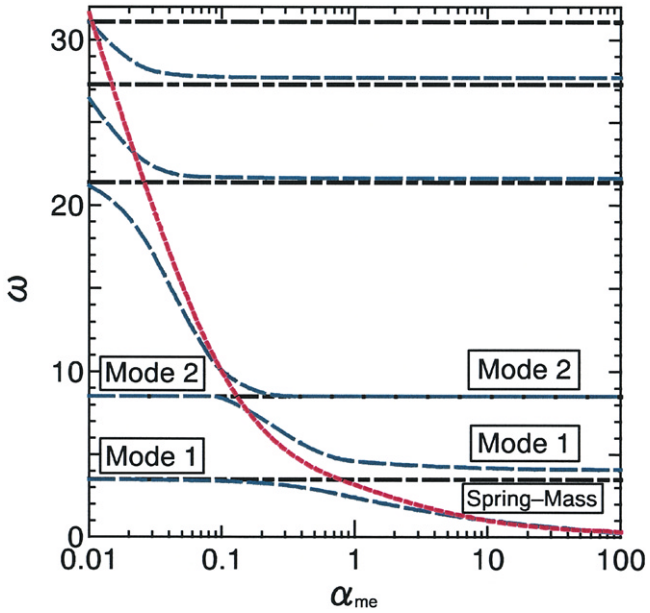

Fig. 18. Natural frequency variation with α_{me}, $\alpha_{ke}=10$, $(\xi_0,\eta_0)=(0.5, 0.5)$.

α_{me}, and aspect ratio λ of the plate, on the vibration characteristics of the coupled system has been clarified. The obtained results from the present paper can be summarized as follows:

(I) Coupled natural frequency

1. Uncoupled natural frequency of the 'spring–mass' system is proportional to $\sqrt{\alpha_{ke}/\alpha_{me}}$.
2. In the left-hand side region of an uncoupled natural frequency curve of the 'spring–mass' system in the $\omega-\alpha_{me}$ diagram, coupled natural frequency is lower than the uncoupled plate frequency, while in the right-hand side of the curve, it is higher, due to the crossing the frequency curves of the uncoupled 'spring–mass' mode and that of the uncoupled plate mode.
3. When one looks at the coupled natural frequencies as Dowell [3], the same conclusion can be obtained as 'if a spring–mass oscillator is attached to another system, a new natural frequency appears between the original pair of frequencies nearest to the oscillator natural frequency'.
4. When the 'spring–mass' is added to a plate just on vibration node at its jth normal mode, coupled jth natural frequency is not changed.

(II) Vibration mode

5. In the vicinity of the natural frequency of the uncoupled 'spring–mass' system, coupled system exhibits motion in which the 'spring–mass' is predominant, while in that of uncoupled plate, coupled system exhibits motion in which the plate motion is predominant. At the crossed region of both curves, strong coupling between the plate motion and the 'spring–mass' motion occurs.

6. When the stiffness parameter α_{ke} becomes large, the effect of spring reduces, and the effect of added mass is significant which constrains the motion of the plate at that point.
7. When the 'spring–mass' is added on the nodal line, there is no effect on the vibration mode of the plate.

(III) Natural frequency ratio depending on attached position

When system parameters lie in the right-hand side of the natural frequency curve of the 'spring–mass' system in the $\omega-\alpha_{me}$ diagram:

8. When the aspect ratio λ is smaller than 1.0, attached position which gives the maximum coupled natural frequency depends on α_{ke}; when α_{ke} is small that point corresponds to the maximum displacement at each vibration mode, while when α_{ke} becomes large it moves from the middle of the free edge to the inward to the clamped side for Mode 1, and moves from free end corners to the clamped side along the free side edge.
   When the aspect ratio λ is larger than 1.0, that point moves from the edge side to the interior of the plate with increase in α_{me} and α_{ke} for Mode 2.
9. Coupled natural frequency ratio mainly depends on α_{ke} than α_{me}.

When only a *mass* is attached on a plate:

10. Letting the spring stiffness approaches infinity reduces the coupled plate frequency due to the added-mass effect.
11. When the aspect ratio is smaller than 1.0, the reduction rate of the plate natural frequency becomes large in Mode 1, while it becomes small in Mode 2, in comparison with that of $\lambda=1.0$. On the other hand, these turns reverse when the aspect ratio becomes larger than 1.0.
12. For Mode 1, with increase in α_{me}, added position which makes minimum natural frequency of the system moves from the free end corner to the clamped side direction along the free edge side. While for Mode 2, this position corresponds to the free end corners when $\alpha_{me}=0.01\sim0.1$, and moves to the free edge side when $\alpha_{me}=1.0$, and moves to the clamped side when $\alpha_{me}=10$, 100.

Appendix A. Derivation of Eq. (15)

Substituting Eq. (10) into Eq. (9), one obtains

$$\tilde{L}=\sum_m\sum_n\sum_r\sum_s a_{mn}a_{rs}\int_0^1\int_0^1\left\{\frac{\partial^2\Phi_m}{\partial\xi^2}\frac{\partial^2\Phi_r}{\partial\xi^2}\Psi_n(\eta)\Psi_s(\eta)+\nu\lambda^2\left(\frac{\partial^2\Phi_m}{\partial\xi^2}\Phi_r(\xi)\Psi_n(\eta)\frac{\partial^2\Psi_s}{\partial\eta^2}+\Phi_m(\xi)\frac{\partial^2\Phi_r}{\partial\xi^2}\frac{\partial^2\Psi_n}{\partial\eta^2}\Psi_s(\eta)\right)+\lambda^4\Phi_m(\xi)\Phi_r(\xi)\frac{\partial^2\Psi_n}{\partial\eta^2}\frac{\partial^2\Psi_s}{\partial\eta^2}+2(1-\nu)\lambda^2\frac{\partial\Phi_m}{\partial\xi}\frac{\partial\Phi_r}{\partial\xi}\frac{\partial\Psi_n}{\partial\eta}\frac{\partial\Psi_s}{\partial\eta}\right\}\mathrm{d}\xi\,\mathrm{d}\eta$$

$$+\alpha_{ke}\lambda\left(b-\sum_m\sum_n a_{mn}\Phi_m(\xi_0)\Psi_n(\eta_0)\right)^2$$
$$-\omega^2\left(\sum_m\sum_n\sum_r\sum_s a_{mn}a_{rs}\int_0^1\int_0^1\Phi_m(\xi)\Psi_n(\eta)\Phi_r(\xi)\Psi_s(\eta)\,\mathrm{d}\xi\,\mathrm{d}\eta+\alpha_{me}b^2\right),$$
$$r=1,2,\ldots,m,\quad s=1,2,\ldots,n, \tag{A.1}$$

$$\tilde{L}=\sum_m\sum_n\sum_r\sum_s a_{mn}a_{rs}\{\alpha_m^4\delta_{mr}\delta_{ns}+\nu\lambda^2(J_{mr}^{20}K_{ns}^{02}+J_{mr}^{02}K_{ns}^{20})+\lambda^4\beta_n^4\delta_{mr}\delta_{ns}+2(1-\nu)\lambda^2J_{mr}^{11}K_{ns}^{11}\}$$
$$+\alpha_{ke}\lambda\left(b^2+2b\sum_m\sum_n a_{mn}\Phi_m(\xi_0)\Psi_n(\eta_0)+\sum_m\sum_n\sum_r\sum_s a_{mn}a_{rs}\Phi_m(\xi_0)\Phi_r(\xi_0)\Psi_n(\eta_0)\Psi_s(\eta_0)\right)$$
$$-\omega^2\left(\sum_m\sum_n\sum_r\sum_s a_{mn}a_{rs}\delta_{mr}\delta_{ns}+\alpha_{me}b^2\right), \tag{A.2}$$

where

$$J_{mr}^{00}=\int_0^1\Phi_m(\xi)\Phi_r(\xi)\,d\xi=\delta_{mr},$$
$$J_{mr}^{11}\equiv\int_0^1\frac{\partial\Phi_m(\xi)}{\partial\xi}\frac{\partial\Phi_r(\xi)}{\partial\xi}\,d\xi=\begin{cases}(3+\alpha_mQ_m)\alpha_mQ_m-\alpha_m\nu_m\mu_m & (m=r),\\ 4(A_{mr}-A_{rm})/(\alpha_m^4-\alpha_r^4) & (m\neq r),\end{cases}$$
$$J_{mr}^{20}\equiv\int_0^1\frac{\partial^2\Phi_m(\xi)}{\partial\xi^2}\Phi_r(\xi)\,d\xi=\begin{cases}(1-\alpha_mQ_m)\alpha_mQ_m+\alpha_m\nu_m\mu_m & (m=r),\\ 4\alpha_mQ_m-4(A_{mr}-A_{rm})/(\alpha_m^4-\alpha_r^4) & (m\neq r),\end{cases}$$
$$A_{mr}=\alpha_m^3\alpha_r(\alpha_mQ_r-\nu_m\alpha_r\mu_r),\quad Q_m=\coth\alpha_m+\cot\alpha_m \tag{A.3}$$

for the integration involving $\Phi_m(\phi)$, where δ_{mr} is Kronecker's delta.

$$K_{ns}^{00}\equiv\int_0^1\Psi_n(\eta)\Psi_n(\eta)\,\mathrm{d}\eta=\delta_{ns},$$
$$K_{ns}^{11}=\int_0^1\frac{\partial\Psi_n(\eta)}{\partial\eta}\frac{\partial\Psi_s(\eta)}{\partial\eta}\,\mathrm{d}\eta=\begin{cases}\beta_n\{3(\bar{Q}_n+\bar{\mu}_n\bar{\nu}_n)+\beta_n\bar{Q}_n^2\} & (n=s),\\ 4(B_{ns}-B_{sn})/(\beta_n^4-\beta_s^4) & (n\neq s),\end{cases}$$
$$K_{ns}^{20}\equiv\int_0^1\frac{\partial^2\Psi_n(\eta)}{\partial\eta^2}\Psi_s(\eta)\,\mathrm{d}\eta=\begin{cases}\beta_n(\bar{Q}_n+\bar{\mu}_n\bar{\nu}_n-\beta_n\bar{Q}_n^2) & (n=s),\\ 4\beta_n(\bar{Q}_n+\bar{\nu}_n\bar{\mu}_n)-4(B_{ns}-B_{sn})/(\beta_n^4-\beta_s^4) & (n\neq s),\end{cases}$$
$$B_{ns}=\beta_n^4\beta_s(\bar{Q}_s+\bar{\mu}_n\bar{\nu}_s),\quad \bar{Q}_n=\coth\beta_n+\cot\beta_n \tag{A.4}$$

for the integration involving $\Psi_n(\eta)$.

Employing the Rayleigh–Ritz method,

$$\frac{\partial\tilde{L}}{\partial a_{mn}}=0,\quad\frac{\partial\tilde{L}}{\partial b}=0 \tag{A.5}$$

yields

$$\frac{\partial \tilde{L}}{\partial a_{mn}} = 2\sum_r \sum_s a_{rs}\{(\alpha_m^4 + \lambda^4\beta_n^4)\delta_{mr}\delta_{ns} + \nu\lambda^2(J_{mr}^{20}K_{ns}^{02} + J_{mr}^{02}K_{ns}^{20}) + 2(1-\nu)\lambda^2 J_{mr}^{11}K_{ns}^{11}\}$$
$$+ \alpha_{ke}\lambda(-2b\sum_m \sum_n \Phi_m(\xi_0)\Psi_n(\eta_0) + 2\sum_r \sum_s a_{rs}\Phi_m(\xi_0)\Phi_r(\xi_0)\Psi_n(\eta_0)\Psi_s(\eta_0))$$
$$- \omega^2(2\sum_r \sum_s a_{rs}\delta_{mr}\delta_{ns}) = 0, \tag{A.6}$$

$$\frac{\partial \tilde{L}}{\partial b} = \alpha_{ke}\lambda\left(2b - 2\sum_m \sum_n a_{mn}\Phi_m(\xi_0)\Psi_n(\xi_0)\right) - \omega^2(2\alpha_{me}b) = 0. \tag{A.7}$$

Appendix B. Nomenclature

a_{nm}, b	unknown constants in Eq. (10)
D	flexural rigidity of plate, $= Eh^3/12(1-\nu^2)$
E	Young's modulus of plate
ν	The Poisson ratio of plate
ρ	mass density of plate
H	width of plate
h	thickness of plate
k_e	attached spring constant
L	length of plate
m_e	attached mass
$W(x, y, t)$	displacement of plate
$\bar{w}$	non-dimensional displacement of plate, $\equiv W/L$
(x, y)	Co-ordinate system
(x_0, y_0)	location of attached 'spring–mass' system
$z(t)$	displacement of spring–mass system
α_{ke}	stiffness ratio parameter, $\equiv k_e L^2/D$
α_m	parameter determined by Eq. (12)
α_{me}	mass ratio parameter, $\equiv m_e/\rho HhL$
β_n	parameter determined by Eq. (14)
λ	aspect ratio of plate, $\equiv L/H$
$\Phi_m(\xi)$	eigenfunction of cantilever beam defined by Eq. (11)
$\Psi_n(\eta)$	eigenfunction of free-free beam defined by Eq. (13)
Ω	natural circular frequency
ω	non-dimensional natural frequency, $\equiv \Omega/\Omega_0$
(ξ, η)	non-dimensional co-ordinate system
Ω_0	natural frequency of plate, $\Omega_0 = \sqrt{D/\rho hL^4}$

References

[1] D. Young, Vibration of beam with concentrated mass, spring, and dashpot, Journal of Applied Mechanics, Trans. ASME 70 (1948) 65–72.
[2] P.A.A. Laura, E.A. Susemihl, J.L. Pombo, L.E. Luisoni, R. Gelos, On the dynamic behaviour of structural elements carrying elastically mounted, concentrated masses, Applied Acoustics 10 (1977) 121–145.
[3] E.H. Dowell, On some general properties of combined dynamical systems, Journal of Applied Mechanics, Trans. ASME 46 (1979) 206–209.
[4] J.W. Nicholson, L.A. Bergman, Free vibration of combined dynamical systems, Journal of Engineering Mechanics 112 (1986) 1–13.
[5] R.E. Rossi, P.A.A. Laura, D.R. Avalos, H. Larrondo, Free vibrations of Timoshenko beams carrying elastically mounted, concentrated masses, Journal of Sound and Vibration 165 (2) (1993) 209–223.
[6] B. Posiadala, Use of Lagrange multiplier formalism to analyze free vibrations of combined dynamical systems, Journal of Sound and Vibration 176 (4) (1994) 563–572.
[7] M. Gürgöze, On the eigenfrequencies of a cantilever beam with attached tip mass and a spring–mass system, Journal of Sound and Vibration 190 (2) (1996) 149–162.
[8] Y.C. Das, D.R. Navakatna, Vibrations of a rectangular plate with concentrated mass, spring, and dashpot, Journal of Applied Mechanics, Trans. ASME 30 (1963) 31–36.
[9] J.C. Snowdon, Vibrations of simply supported rectangular and square plates to which lumped masses and dynamic vibration absorbers are attached, Journal of Acoustical Society of America 57 (3) (1975) 646–654.
[10] J.W. Nicolson, L.A. Bergman, Vibration of damped plate–oscillator systems, Journal of Engineering Mechanics 112 (1) (1986) 14–30.
[11] D. Trentin, J.L. Gulader, Vibrations of a master plate with attached masses using modal sampling method, Journal of Acoustical Society of America 96 (1) (1994) 235–245.
[12] E.H. Dowell, D. Tang, The high-frequency response of a plate carrying a concentrated mass/spring system, Journal of Sound and Vibration 213 (5) (1998) 843–863.
[13] P.D. Cha, W.C. Wong, A novel approach to determine the frequency equations of combined dynamical systems, Journal of Sound and Vibration 219 (4) (1999) 689–706.
[14] K.-M. Won, Y.-S. Park, Optimal support position for a structure to maximize its fundamental natural frequency, Journal of Sound and Vibration 213 (5) (1998) 801–812.
[15] A.W. Leissa, On a curve veering aberration, Journal of Applied Mathematics and Physics 25 (1974) 99–111.
[16] N.C. Perkins, C.D. Mote Jr., Comments on curve veering in eigenvalue problem, Journal of Sound and Vibration 106 (3) (1986) 451–463.
[17] M. Chiba, I. Yoshida, Free vibration of a rectangular plate–beam coupled system, Journal of Sound and Vibration 194 (1) (1996) 49–65.